Directional Control of Transient Flows Generated by Thermoplasmonic Bubble Nucleation

THE JOURNAL OF PHYSICAL CHEMISTRY C
A JOURNAL OF THE AMERICAN CHEMICAL SOCIETY

pubs.acs.org/JPCC
Article

Directional Control of Transient Flows Generated by Thermoplasmonic Bubble Nucleation

Pantea Dara, Mahdi Shanei, Steven Jones, and Mikael Käll*

Cite This: J. Phys. Chem. C 2023, 127, 17454−17459
Read Online

ACCESS | Metrics & More | Article Recommendations | Supporting Information

ABSTRACT: It has previously been shown that strong flow transients, reaching mm/s flow speeds, are induced when microscopic vapor bubbles nucleate on spatially isolated laser-heated plasmonic nanoantennas supported on a substrate. However, the flow pattern is cylindrically symmetric and always directed toward the nanoantenna at the substrate plane. This limits its applicability in, for example, particle manipulation schemes. Here, we show that the flow direction can be locally reversed by breaking the photothermal symmetry using two nearby nanoantennas that differ either in size or polarization response. The in-plane flow transient is strong enough to push microparticles tens of microns across a surface. Directional flow control may provide the means for rapid and precise mass transport near surfaces for applications in microfluidics, bionanotechnology, and particle sorting.

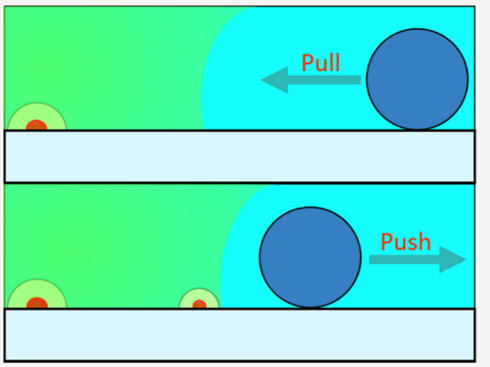

INTRODUCTION

Optical control over fluid flows has been explored as a flexible "contact-free" complement or alternative to conventional microfluidic manipulation for various applications, including surface-based biomolecular sensing,[1,2] positioning and guiding of nanostructures,[3,4] and physical deposition.[5,6] One promising method for generating localized flow via external illumination is to utilize photothermally induced vapor bubbles created at a water−solid interface supporting gold nanoparticles. Because of the enhanced optical absorption associated with the localized surface plasmon resonance phenomenon, the chemically inert gold nanoparticles will act as effective nanoscopic optical antennas able to rapidly superheat and vaporize the surrounding water into a microscopic bubble.[7−9] The thermal surface tension gradient on the liquid−vapor interface thus created, in turn, drives localized fluid flow due to the Marangoni effect,[10,11] thereby providing an effective route toward optothermal manipulation at the micrometer scale.

Several proof-of-principle applications based on bubble-induced flow have been demonstrated, such as increasing the detection rate of surface-based sensors[12,13] and manipulating nanostructures.[14,15] However, in most of these studies, the created bubbles were tens to hundreds of microns in size. Such large bubbles do not allow for rapid and dynamic flow control because of the diffusion limited slow expulsion of dissolved gas, accumulated in the bubble from the surrounding water, after illumination has ceased.[16,17] Though the bubble lifetime can be decreased by using degassed water,[18,19] this is not feasible in most practical applications.[18,20] As a solution to this issue, Jones et al. recently demonstrated that spatially isolated gold nanoantennas are able to produce micron-sized bubbles that can be modulated at up to kHz frequencies in air-equilibrated water.[21,22] The reason for this is that it is now the spatial extension of the plasmonic antenna that determines the bubble size rather than the illuminated area, as in previous experiments with distributed plasmonic arrays.[23−25] Furthermore, it was found that a very strong transient, producing mm/s flow velocities close to the antenna, is induced as a microbubble form.[22] The origin of the transient is not completely understood, but it is likely to at least partly be due to the pressure emitted when a bubble nucleates and rapidly expands from the surface of a gold nanoparticle.[26,27]

Regardless of the detailed origin of the flow transient, it was found that its vectorial flow profile, schematically illustrated in Figure 1a, was the same as that of the subsequent persistent Marangoni flow and directed *toward* the bubble at the interface supporting the antenna structure.[22] However, to utilize the strong transient in applications such as particle manipulation, it would be highly advantageous to also be able to induce an *outward* shear flow such that particles could be pushed away from the microbubble. Here, we show that this is possible by breaking the in-plane cylindrical symmetry of the single microbubble. As indicated in Figure 1b, we achieved this by illuminating two nearby antenna structures with different optical absorption efficiency such that two unequal micro-

Received: April 5, 2023
Revised: August 10, 2023
Published: August 28, 2023

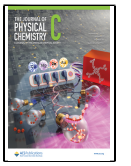

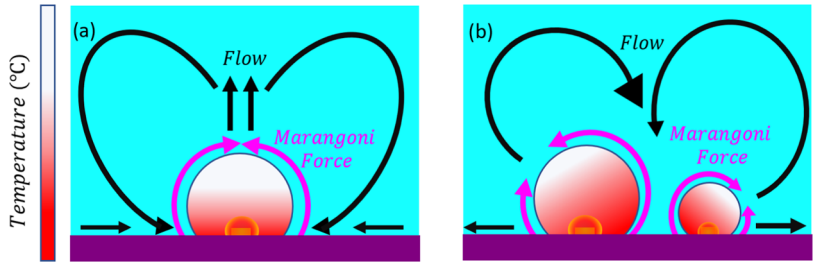

Figure 1. Expected Marangoni flow induced by (a) a single bubble with a temperature gradient normal to the interface and (b) by two unequal nearby bubbles with an additional temperature gradient parallel to the surface.

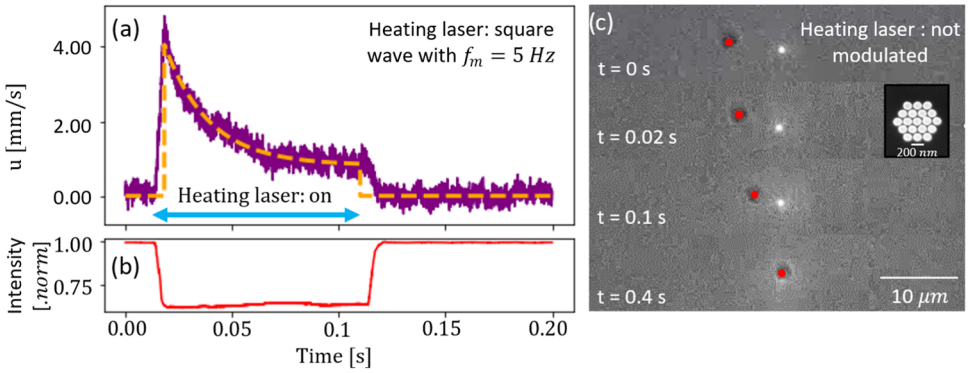

Figure 2. (a) Optical force measurement of flow amplitude versus time (violet curve) near a single antenna during one cycle of 532 nm laser illumination modulated as a square wave with frequency f_m = 5 Hz and peak intensity of ~4.4·10^3 W/cm^2. The flow is well approximated by the sum of an exponentially decaying transient and a constant flow term (orange dashed curve). (b) Red curve shows the transmission of the 632 nm probe beam used to qualitatively record the bubble dynamics. Low transmission implies that a bubble is present on the gold antenna. (c) Video grabs showing a 2 μm probe particle (indicated by a red dot) as it is pulled toward a single antenna by the bubble-induced flow. The probe is settled on the interface supporting the antenna, which is visible as a small white dot. The inset shows a scanning electron micrograph of the antenna, which consists of a hexagonal array of 100 nm diameter, 60 nm tall gold disks with center-to-center spacing of 150 nm.

bubbles were simultaneously generated by the incident light field. This idea is inspired by recent results from Namura and co-workers, who found that it was possible to control the flow direction through an in-plane temperature gradient created by using either two nearby illumination spots applied to a uniform plasmonic substrate[23] or by illuminating a single elongated and asymmetric gold microparticle.[28] Both these investigations utilized degassed water and involved stationary Marangoni flows driven by ~10 μm diameter vapor bubbles.[23,28]

METHODS

The sample layout, measurement methodology, and simulation approach essentially follow Jones et al.[21,22] and are further detailed in the Supporting Information (SI). In brief, we used photothermal antennas in the form of 60 nm thin gold disks or ellipsoids arranged in small hexagonal arrays on a glass substrate for bubble generation. Each antenna acts as an essentially independent heat source, such that the total number of antennas in an array determines the net heat production for uniform illumination. The antennas were situated in a ~120 μm thin liquid cell filled with air-equilibrated water and excited by a defocused laser beam (λ = 532 or 660 nm) modulated in a square wave temporal profile (duty cycle = 50%) with frequency f_m. Bubble formation and subsequent temporal dynamics of a single bubble can be qualitatively tracked by monitoring the transmission of a low-power 632 nm beam focused on the antenna structure. We used optical force microscopy, based on a holographic optical tweezers system operated at 1064 nm, to quantify the force $\boldsymbol{F}(\boldsymbol{r},t)$ acting on a 2 μm diameter polystyrene (PS) probe particle trapped near an antenna. The force was then converted to a flow speed $\boldsymbol{u}(\boldsymbol{r},t)$ by dividing with the relevant Stokes drag coefficient for translation near a no-slip interface. We additionally tracked the movement of probe particles settled on the substrate using video microscopy as a complementary method to visualize particle manipulation near an interface.

RESULTS AND DISCUSSION

Figure 2a illustrates the temporal variation of the flow amplitude $u(t)$ recorded near an antenna with structure parameters designed to enable the generation of small bubbles with short lifetimes.[21] As discussed in ref 22, the behavior can be characterized as a strong but short-lived transient response associated with the bubble nucleation and expansion process, followed by a weak and slowly decaying "persistent" Marangoni flow. The time dependence can be quite well described as the sum of an exponential decay with an initial amplitude u_t and a constant term with amplitude u_p, $u(t) = \Theta(t - t_0)[u_t \exp(-t/\tau) + u_p]$, where the step function Θ indicates the onset of illumination at t_0. The transient decay time τ is of the order 20 ms while the time it takes for the flow to cease after illumination has stopped, indicating the bubble "lifetime," is of the order 1 ms for the structure sizes and illumination intensities used here.[21]

As mentioned in the Introduction section and illustrated in Figure 1a, a bubble induced on a single circularly symmetric antenna generates a flow directed radially inward at the supporting interface. Figure 2c illustrates the effect this flow

https://doi.org/10.1021/acs.jpcc.3c02263
J. Phys. Chem. C 2023, 127, 17454−17459

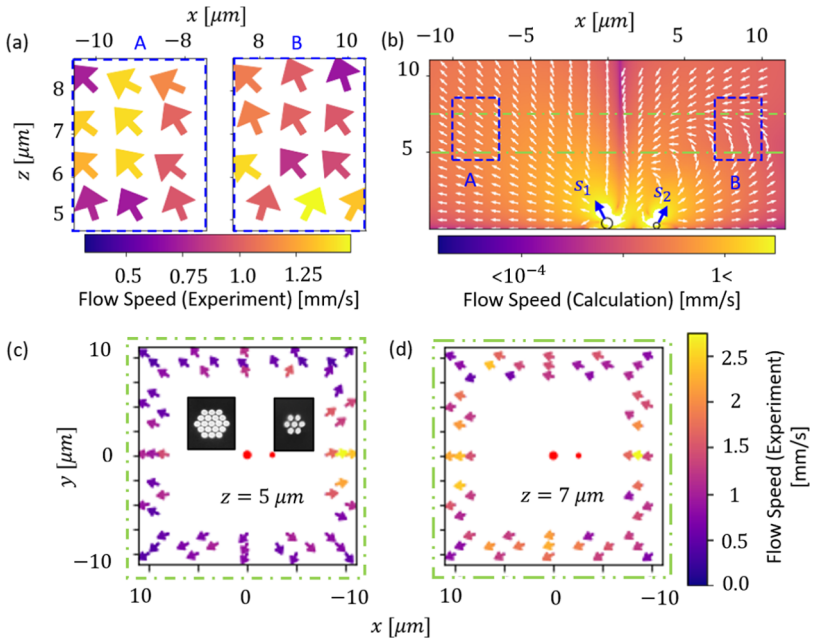

Figure 3. Measured bubble-induced flow transient vectors around an asymmetric pair of antennas spaced 2 μm apart (a) in the *xz*-plane (indicated by blue boxes A and B); (c) and (d) in the xy-plane at z = 5 and 7 μm from the interface (indicated by green dashed lines). The arrows show the projection of the flow vectors on the *xz*- and *xy*-planes, respectively, while the total flow magnitudes are indicated in color. The measured flows are well approximated by a calculation (shown in b) based on two tilted Stokeslets with relative amplitudes and inclination angles as indicated by blue arrows S_1 and S_2. Insets in panel (c) show SEM micrographs of the primary and secondary antenna structures, consisting of 19 and 7 gold disks, respectively. The flow transient was induced by a 532 nm laser beam ($w_0 \approx 27$ μm, $P \approx 50$ mW) centered on the primary antenna structure and modulated as a square wave with a frequency f_m = 5 Hz. Note that the flow is directed radially outward from the antennas at the plane closest to the interface and that the *y*-component of the flow near the secondary antenna reverts in the higher planes.

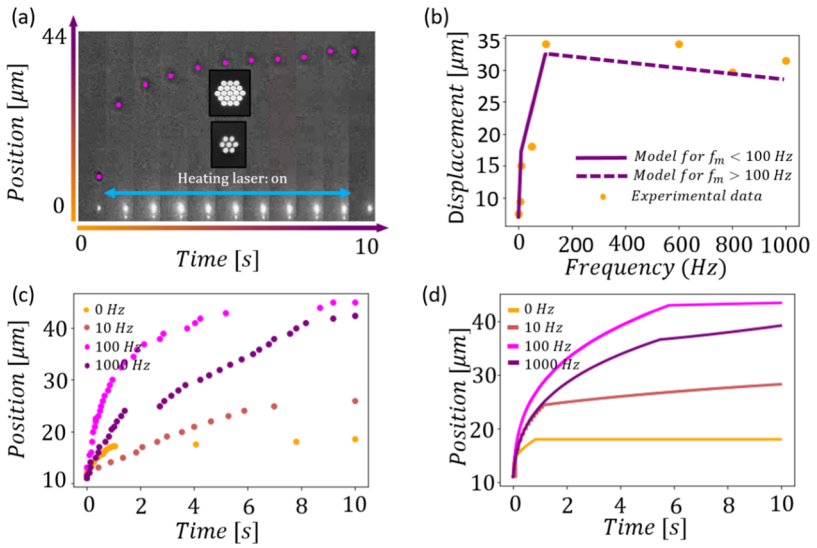

Figure 4. Tracking of probe particles subject to transient flows produced by bubbles on an asymmetric pair of antennas. (a) Video grabs showing a 2 μm probe (violet dot) settled on the interface as it is pushed away from the antenna pair by the bubble-induced flow. The antenna pair is visible as two bright white dots at the bottom of the figure. The heating laser is modulated at a frequency of f_m = 100 Hz. (b) Total experimental (dots) and simulated (line) probe displacement versus modulation frequency f_m = 0 to 1 kHz. (c) Probe position versus time for four selected modulation frequencies. (d) Simulated probe position versus time for the same modulation frequencies as in panel (c). The antenna structure parameters and illumination conditions were the same as in Figure 3.

has on a probe particle settled on the glass substrate. Despite the reduced flow speed resulting from the no-slip boundary condition at the interface, the particle is gradually pulled toward the antenna, where it is eventually trapped. The particle may diffuse away if illumination ceases, but it is obviously impossible to actively manipulate the particle's radial position without the ability to also generate flow in the opposite direction. To investigate this possibility, we study the flow induced by a pair of unequal nearby antennas.

Figure 3 summarizes results for a pair consisting of a primary antenna formed by 19 nanodisks, as shown in Figure 2c, and a secondary antenna of 7 disks at an edge-to-edge distance of d =

https://doi.org/10.1021/acs.jpcc.3c02263
J. Phys. Chem. C 2023, 127, 17454−17459

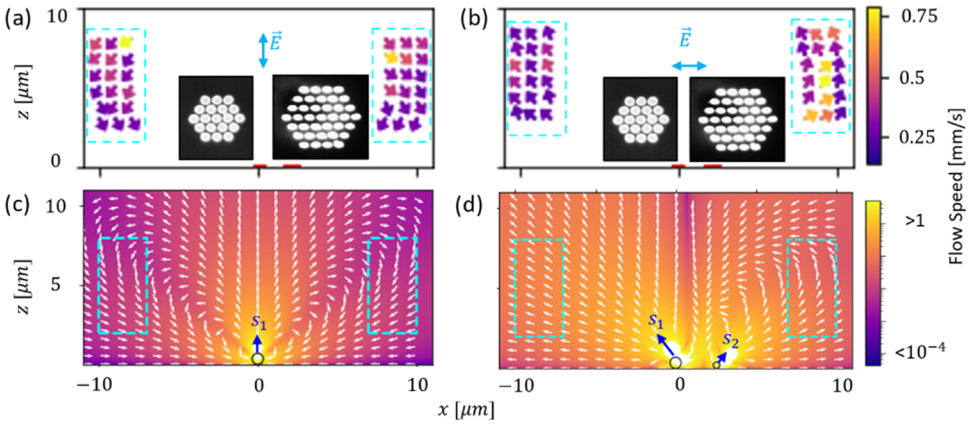

Figure 5. Polarization-dependent bubble-induced flow transients around an asymmetric pair of antennas spaced 2 μm apart. The polarization-insensitive primary antenna is of the same type as used in Figures 3 and 4, while the secondary antenna, constructed from 37 ellipsoidal nanodisks, exhibits highly polarization-dependent light absorption at the heating laser wavelength used (λ = 660 nm). Panels (a) and (b) show measured transient flow in the *xz*-plane for incident polarization perpendicular and parallel to the ellipsoidal long axis, respectively. The flow profiles within the regions indicated by blue boxes are well approximated by calculations based on (c) either one vertical Stokeslet (S_1) or (d) two tilted Stokeslets (S_1 and S_2). The 660 nm heating laser beam ($w_0 \approx 32$ μm, $P \approx 50$ mW, $f_m = 5$ Hz) was centered on the major antenna structure. Note the change in flow direction as polarization shifts from perpendicular to parallel.

2 μm. The sizes and structure of the antenna arrays were chosen based on the results reported in ref 21 and ensure rapid bubble modulation for the laser intensities available in our experimental system. The chosen antenna spacing was found to be large enough to prevent the formation of a single large bubble covering both antennas yet small enough to generate the thermal gradient required for generating an outward flow. The pair is photothermally excited by a laser beam (λ = 532 nm, P_{532} = 50 mW) with a large beam waist ($w_0 \approx 27$ μm) such that both antennas receive approximately the same irradiance. We perform flow velocimetry based on optical force microscopy for a heating laser modulation frequency of f_m = 5 Hz. We plot the maximum flow speed, corresponding to the transient response, within selected planes near the antennas. As is particularly evident from the *xy*-plane data recorded at z = 5 μm, the flow has now indeed acquired a substantial component directed away from the antennas near the interface. However, because of mass conservation, this outward-directed flow needs to revert toward the antennas in some regions of space. We cannot measure directly above the antennas, where this effect should be most pronounced, but a clear reversal of the lateral flow component is evident from the data recorded 7−8 μm from the interface near the secondary antenna.

We use the Stokeslet approximation to interpret the measurement data and to obtain a clearer picture of the overall flow profile. As shown by Namura et al.,[23,25] this model can successfully simulate bubble-induced flows near an interface when expanded to incorporate a no-slip (zero velocity) boundary condition.[29] The direction of the Stokeslet force singularity indicates the direction of the temperature gradient on the bubble surface, that is, normal to the interface for a single symmetric bubble but "tilted" if a lateral thermal gradient exists.[23,25] In the present case, we were not able to simulate the flow pattern using a single Stokeslet, regardless of its tilt angle. However, if we use two such tilted Stokeslets, representing two bubbles located at the position of the primary and the secondary antenna, respectively, it is possible to qualitatively reproduce the experimentally recorded flow pattern very well. As indicated in Figure 3, the Stokeslets need to tilt away from the pair's center, reflecting the higher temperature on the part of a bubble surface that faces the neighboring antenna. Good quantitative agreement is found for a tilt angle of 45° and by positioning the point forces ∼0.7 μm above the interface, reflecting the approximate size of a microbubble (see the SI for details).

The data in Figure 3 suggests that the microbubble flow transients can push a particle across the interface away from the asymmetric antenna pair, as schematically indicated in Figure 1b. To test this experimentally, we tracked the trajectory of individual probe particles free to move on the surface. The measurements, summarized in Figure 4, were performed by first placing a probe ∼11 μm from the primary antenna in the direction of the pair axis, using the optical tweezers. The tweezers were then turned off and the 532 nm heating laser turned on, after which the probe was video tracked for ∼10 s at a frame rate of ∼10 Hz. Measurements were performed for heating modulation frequencies varying from f_m = 0 to 1 kHz.

Figure 4a shows video grabs during the translation experiment run at f_m = 100 Hz, demonstrating a rapid outward particle displacement, as anticipated from the flow pattern in Figure 3. The initial particle speed is ∼200 μm/s, gradually decreasing until movement stops due to stiction at ∼45 μm from the primary antenna. Figure 4b shows total displacement vs f_m, while Figure 4c plots displacement vs time for four selected frequencies. These data clearly demonstrate the crucial importance of the flow transient. For f_m = 0 Hz, for which there is only one transient (at t = 0) but twice the integrated laser power, the probe ceases to move already ∼17 μm from the primary antenna (see Supporting Figure S5 for a comparison of the particle speed and simulated flow speed for this case). The total displacement and average initial speed then increase gradually with modulation frequency up to the optimum case of f_m = 100 Hz, after which a slight decrease occurs when the bubble no longer has time to fully dissipate during the"dark" intervals between the illumination sequences.[22] These trends can be qualitatively captured by a crude model based on the exponential decrease in flow speed after bubble nucleation illustrated in Figure 2a. We here assume that the probe moves with the same speed as the flow but that there

https://doi.org/10.1021/acs.jpcc.3c02263
J. Phys. Chem. C 2023, 127, 17454−17459

is a minimum flow speed, here set to 3.3 μm/s, required for movement due to stiction between the probe and the substrate interface. Further, we assume that the flow speed decreases with distance r from the primary antenna as r^{-3}, as indicated by the Stokeslet calculation (see Figure S4 in the Supporting Information). The particle speed during one heating cycle is thus modeled as $u(t,r) = [u_t \exp(-t/\tau) + u_p](r/r_0)^{-3}$, which can then be integrated over all heating cycles in an illumination sequence to generate overall displacement vs time. As shown in Figure 4b,d, the simple model with u_t = 4 mm/s, u_p = 0.2 mm/s, τ = 20.9 ms, and r_0 = 4.24 μm describes the data quite well up to f_m = 100 Hz. However, for higher modulation frequencies, we find that a model that disregards the transient response, i.e., $u(t, r) = u_p(r/r_0)^{-3}$ with u_p = 3 mm/s is adequate. This can be understood by the fact that a microbubble needs some time to completely dissipate during the dark intervals in an illumination sequence. Thus, if the bubble lifetime becomes comparable to or longer than $1/2f_m$, the magnitude of the bubble transient u_t decreases gradually, eventually resulting in a static Marangoni flow.

As a final investigation, we tried to dynamically control the flow direction by altering the polarization of the heating laser. To obtain the desired polarization dependence, we designed the secondary antenna from 100 nm x 50 nm ellipsoidal gold nanodisk while the primary antenna and the antenna spacing were kept, as shown in Figure 4. By changing the heating laser wavelength to λ = 660 nm, we maximized the polarization-independent heating of the primary antenna while the secondary antenna only heated well for polarization parallel to the long axis of the ellipsoids (Figure S1).[30] We would thus expect a symmetric flow pattern (as shown in Figure 1a) for perpendicular polarization and an asymmetric pattern (as shown in Figures 1b and 3) for the parallel case, implying a reversed flow direction at the interface.

Figure 5 summarizes flow data and calculations for the two polarization configurations. For the case when polarization is perpendicular to the ellipsoidal long axis, that is, when only the primary antenna is expected to heat significantly, the flow pattern is essentially symmetric and directed toward the antenna pair near the interface. The flow is thus similar to that generated by a single bubble, indicating that the net light absorption generated in the secondary antenna is below the threshold for bubble generation in this case. Consequently, the flow pattern is well represented by a single vertically oriented Stokeslet. However, the flow pattern completely reverts direction when polarization is turned parallel. Light absorption in the secondary antenna is now sufficient for bubble generation, resulting in a flow pattern analogous to that shown in Figure 3 and represented by two tilted Stokeslets.

Finally, we performed finite element (FEM) simulations of equilibrium flows and thermal distributions as an independent validity check of the results above. These calculations, which are summarized in Supporting Information Figures S5 and S6, are based on realistic photothermal heat source densities, bubble sizes, and surface tension coefficients. All in all, the FEM simulated flow patterns turn out to be in excellent agreement with the experimental results and Stokeslet simulations shown in Figures 3 and 5. However, this agreement could only be reached if the centers of the bubbles, which were modeled as half-spheres, were shifted to the outer edges of the antenna arrays. Such a shift, which amplifies the thermal gradients on the bubble surfaces, is plausible given that the outward-directed flows in the measurement regions outside the antennas must be compensated by a similar flow in the region between the antennas, which would tend to push the bubbles toward the outer edges of the antenna arrays (see Supporting Figure S8). A second notable difference is that the calculated flow speeds are significantly lower than measured, but this is expected, considering that the FEM model assumes equilibrium conditions and neglects the transient response. The FEM simulations indicate that the surface temperature of the gold nanoparticles reaches more than 200 °C at equilibrium but decays to room temperature within a few μm from the antenna arrays, which is in good agreement with previous studies of bubble formation on nanoplasmonic structures.[16]

SUMMARY AND CONCLUSIONS

In summary, we showed that it is possible to revert the transient flow associated with vapor bubble nucleation on photothermally excited gold nanoantennas by creating an in-plane thermal gradient across the bubble surface. The thermal gradient was created by illuminating two closely spaced dissimilar antennas, each supporting a microscopic vapor bubble, using a single laser beam. Experimentally recorded flow patterns could be qualitatively reproduced in calculations based on two tilted Stokeslets, as well as by finite element simulations. Further, we found that the transient flows were strong enough to push a microparticle, settled on the substrate, over tens of microns away from the nanoantennas within a few seconds. Finally, by constructing one of the antennas in a pair from ellipsoidal gold particles, we showed that the transient flow direction could be reversed by changing the polarization of the incident illumination.

Significant effort has been made over the past decades to develop microfluidic geometries that enable mixing multiple streams, selective focusing of particles, etc. The results discussed here demonstrate that photothermal bubble nucleation on designed nanostructures can be used as an effective means of generating local flows and fluidic forces with a high degree of directional and temporal control in a microfluidic environment. We believe that this concept could be further developed as a fundamental basis for advanced "active" microfluidic systems that are not limited by the constraints of chamber geometry or input/output pressure differential. Such systems are envisioned to have applications in diagnostic sensing devices, for example, to act as an accumulator of analytes or to selectively mix from multiple chambers.

ASSOCIATED CONTENT

Supporting Information

The Supporting Information is available free of charge at https://pubs.acs.org/doi/10.1021/acs.jpcc.3c02263.

Samples and fabrication; experimental setup; flow measurement procedures, Stokeslet simulation details, and finite element flow simulations (PDF)

AUTHOR INFORMATION

Corresponding Author

Mikael Käll − *Department of Physics, Chalmers University of Technology, 41296 Gothenburg, Sweden;* orcid.org/0000-0002-1163-0345; Email: mikael.kall@chalmers.se

https://doi.org/10.1021/acs.jpcc.3c02263
J. Phys. Chem. C 2023, 127, 17454−17459

Authors

Pantea Dara − *Department of Physics, Chalmers University of Technology, 41296 Gothenburg, Sweden;* orcid.org/0000-0002-4536-193X

Mahdi Shanei − *Department of Physics, Chalmers University of Technology, 41296 Gothenburg, Sweden;* orcid.org/0000-0001-9099-0711

Steven Jones − *Department of Physics, Chalmers University of Technology, 41296 Gothenburg, Sweden;* Present Address: TTP - The Technology Partnership, SG8 6HQ Melbourn, England

Complete contact information is available at: https://pubs.acs.org/10.1021/acs.jpcc.3c02263

Author Contributions

The manuscript was written through contributions of all authors. All authors have given approval to the final version of the manuscript.

Notes

The authors declare no competing financial interest.

■ ACKNOWLEDGMENTS

This work was supported by the Swedish Research Council and the Knut and Alice Wallenberg Foundation. Nanofabrication was conducted at Myfab Chalmers.

■ REFERENCES

(1) Chen, J.; Zeng, Y.; Zhou, J.; Wang, X.; Jia, B.; Miyan, R.; Zhang, T.; Sang, W.; Wang, Y.; Qiu, H.; et al. Optothermophoretic Flipping Method for Biomolecule Interaction Enhancement. *Biosens. Bioelectron.* **2022**, *204*, No. 114084.

(2) Hong, C.; Yang, S.; Ndukaife, J. C. Stand-Off Trapping and Manipulation of Sub-10 nm Objects and Biomolecules Using Opto-Thermo-Electrohydrodynamic Tweezers. *Nat. Nanotechnol.* **2020**, *15*, 908−913.

(3) Fränzl, M.; Cichos, F. Hydrodynamic Manipulation of Nano-Objects by Optically Induced Thermo-Osmotic Flows. *Nat. Commun.* **2022**, *13*, No. 656.

(4) Rodrigo, J. A.; Angulo, M.; Alieva, T. Tailored Optical Propulsion Forces for Controlled Transport of Resonant Gold Nanoparticles and Associated Thermal Convective Fluid Flows. *Light Sci. Appl.* **2020**, *9*, No. 181.

(5) Lin, L.; Peng, X.; Zheng, Y. Reconfigurable Opto-Thermoelectric Printing of Colloidal Particles. *Chem. Commun.* **2017**, *53*, 7357−7360.

(6) Tekin, E.; Smith, P. J.; Schubert, U. S. Inkjet Printing as a Deposition and Patterning Tool for Polymers and Inorganic Particles. *Soft Matter* **2008**, *4*, 703−713.

(7) Baffou, G. *Thermoplasmonics: Heating Metal Nanoparticles Using Light*; Cambridge University Press: Cambridge, 2017.

(8) Lombard, J.; Biben, T.; Merabia, S. Kinetics of Nanobubble Generation around Overheated Nanoparticles. *Phys. Rev. Lett.* **2014**, *112*, No. 105701.

(9) Xie, Y.; Zhao, C. An Optothermally Generated Surface Bubble and Its Applications. *Nanoscale* **2017**, *9*, 6622−6631.

(10) Chikazawa, J. I.; Uwada, T.; Furube, A.; Hashimoto, S. Flow-Induced Transport via Optical Heating of a Single Gold Nanoparticle. *J. Phys. Chem. C* **2019**, *123*, 4512−4522.

(11) Setoura, K.; Ito, S.; Miyasaka, H. Stationary Bubble Formation and Marangoni Convection Induced by CW Laser Heating of a Single Gold Nanoparticle. *Nanoscale* **2017**, *9*, 719−730.

(12) Karim, F.; Sun, Y.; Vasquez, E. S.; Zhao, C. Active and Ultrasensitive Chemical and Biosensing through Optothermally Generated Microbubble In *Conference on Lasers and Electro-Optics*; Optica Publishing Group: Washington, DC, 2020.

(13) Kim, Y.; Ding, H.; Zheng, Y. Enhancing Surface Capture and Sensing of Proteins with Low-Power Optothermal Bubbles in a Biphasic Liquid. *Nano Lett.* **2020**, *20*, 7020−7027.

(14) Bangalore Rajeeva, B.; Lin, L.; Perillo, E. P.; Peng, X.; Yu, W. W.; Dunn, A. K.; Zheng, Y. High-Resolution Bubble Printing of Quantum Dots. *ACS Appl. Mater. Interfaces* **2017**, *9*, 16725−16733.

(15) Zheng, Y.; Liu, H.; Wang, Y.; Zhu, C.; Wang, S.; Cao, J.; Zhu, S. Accumulating Microparticles and Direct-Writing Micropatterns Using a Continuous-Wave Laser-Induced Vapor Bubble. *Lab Chip* **2011**, *11*, 3816−3820.

(16) Baffou, G.; Polleux, J.; Rigneault, H.; Monneret, S. Super-Heating and Micro-Bubble Generation around Plasmonic Nanoparticles under cw Illumination. *J. Phys. Chem. C* **2014**, *118*, 4890−4898.

(17) Li, J.; Zhao, F.; Deng, Y.; Liu, D.; Chen, C. H.; Shih, W. C. Photothermal Generation of Programmable Microbubble Array on Nanoporous Gold Disks. *Opt. Express* **2018**, *26*, 16893−16902.

(18) Wang, Y.; Zaytsev, M. E.; Lajoinie, G.; The, H. L.; Eijkel, J. C.; van den Berg, A.; Versluis, M.; Weckhuysen, B. M.; Zhang, X.; Zandvliet, H. J.; Lohse, D. Giant and Explosive Plasmonic Bubbles by Delayed Nucleation. *Proc. Natl. Acad. Sci. U.S.A.* **2018**, *115*, 7676−7681.

(19) Wang, Y.; Zaytsev, M. E.; The, H. L.; Eijkel, J. C.; Zandvliet, H. J.; Zhang, X.; Lohse, D. Vapor and Gas-Bubble Growth Dynamics around Laser-Irradiated, Water-Immersed Plasmonic Nanoparticles. *ACS Nano* **2017**, *11*, 2045−2051.

(20) Liu, X.; Bao, L.; Dipalo, M.; De Angelis, F.; Zhang, X. Formation and Dissolution of Microbubbles on Highly-Ordered Plasmonic Nanopillar Arrays. *Sci. Rep.* **2016**, *5*, No. 18515.

(21) Jones, S.; Andrén, D.; Antosiewicz, T. J.; Käll, M. Ultrafast Modulation of Thermoplasmonic Nanobubbles in Water. *Nano Lett.* **2019**, *19*, 8294−8302.

(22) Jones, S.; Andrén, D.; Antosiewicz, T. J.; Stilgoe, A.; Rubinsztein-Dunlop, H.; Käll, M. Strong Transient Flows Generated by Thermoplasmonic Bubble Nucleation. *ACS Nano* **2020**, *14*, 17468−17475.

(23) Namura, K.; Imafuku, S.; Kumar, S.; Nakajima, K.; Sakakura, M.; Suzuki, M. Direction Control of Quasi-Stokeslet Induced by Thermoplasmonic Heating of a Water Vapor Microbubble. *Sci. Rep.* **2019**, *9*, No. 4770.

(24) Namura, K.; Nakajima, K.; Kimura, K.; Suzuki, M. Photothermally Controlled Marangoni Flow around a Micro Bubble. *Appl. Phys. Lett.* **2015**, *106*, No. 043101.

(25) Namura, K.; Nakajima, K.; Suzuki, M. Quasi-Stokeslet Induced by Thermoplasmonic Marangoni Effect around a Water Vapor Microbubble. *Sci. Rep.* **2017**, *7*, No. 45776.

(26) Lombard, J.; Lam, J.; Detcheverry, F.; Biben, T.; Merabia, S. Strong and Fast Rising Pressure Waves Emitted by Plasmonic Vapor Nanobubbles. *Phys. Rev. Res.* **2021**, *3*, No. 023231.

(27) Hou, L.; Yorulmaz, M.; Verhart, N. R.; Orrit, M. Explosive Formation and Dynamics of Vapor Nanobubbles around a Continuously Heated Gold Nanosphere. *New J. Phys.* **2015**, *17*, No. 013050.

(28) Namura, K.; Hanai, S.; Kondo, S.; Kumar, S.; Suzuki, M. Gold Micropetals Self-Assembled by Shadow-Sphere Lithography for Optofluidic Control. *Adv. Mater.* **2022**, *9*, No. 2200200.

(29) Blake, J. R.; Chwang, A. T. Fundamental Singularities of Viscous Flow. *J. Eng. Math* **1974**, *8*, 23−29.

(30) Girard, C.; Wiecha, P. R.; Cuche, A.; Dujardin, E. Designing Thermoplasmonic Properties of Metallic Metasurfaces. *J. Opt.* **2018**, *20*, No. 075004.